Supplement of Atmos. Chem. Phys., 19, 10405–10422, 2019
https://doi.org/10.5194/acp-19-10405-2019-supplement

Atmospheric Chemistry and Physics
Open Access
EGU

Supplement of

High contributions of fossil sources to more volatile organic aerosol

Haiyan Ni et al.

Correspondence to: Ru-Jin Huang (rujin.huang@ieecas.cn)

S1. Stable carbon isotopic composition of EC

The stable carbon isotopic composition of EC was determined using a Finnigan MAT 251 mass spectrometer with a dual inlet system (Bremen, Germany) at the Stable Isotope Laboratory at the Institute of Earth Environment, Chinese Academy of Sciences. OC is removed by heating the filter pieces at 375 °C for 3 h in a vacuum-sealed quartz tube in the presence of CuO catalyst grains. Extraction of EC was done by heating the carbon that remained on the filters at 850 °C for 5 h. The evolved CO_2 from EC was isolated by a series of cold traps and quantified manometrically. The stable carbon isotopic composition of the purified CO_2 of EC was measured and determined as $\delta^{13}C_{EC}$. A routine laboratory working standard with a known $\delta^{13}C$ value was measured every day. The quantitative levels of ^{13}C and ^{12}C isotopes were characterized using a ratio of peak intensities of m/z 45 ($^{13}C^{16}O_2$) and 44 ($^{12}C^{16}O_2$) in the mass spectrum of CO_2. Samples were analyzed at least in duplicate, and all replicates showed differences less than 0.3 ‰. $\delta^{13}C$ values are reported in the delta notation with respect to the international standard Vienna Pee Dee Belemnite (V-PDB):

$$\delta^{13}\mathrm{C}\ (‰) = \left[\frac{\left(^{13}\mathrm{C}/^{12}\mathrm{C}\right)_{\mathrm{sample}}}{\left(^{13}\mathrm{C}/^{12}\mathrm{C}\right)_{\mathrm{V-PDB}}} - 1\right] \times 1000. \quad \text{(S1)}$$

Details of stable carbon isotope measurements are described by our previous studies (Cao et al., 2011; Ni et al., 2018).

S2. Separation of fossil sources into coal and vehicle for EC using Bayesian statistics

Contributions from biomass burning and fossil sources to EC is separated by $F^{14}C_{EC}$ (Sect. 2.4). The relative contribution of fossil fuel combustion to EC (f_{fossil}(EC)) and biomass burning to EC (f_{bb}(EC)) constrained by $F^{14}C_{EC}$ is shown in Table S5. f_{fossil}(EC) can be further separated into the fraction of EC contributed by coal combustion(f_{coal}) and vehicle emissions ($f_{vehicle}$) using $\delta^{13}C$ of EC in a Bayesian Markov chain Monte Carlo (MCMC) scheme:

$$\delta^{13}\mathrm{C}_{\mathrm{EC}} = \delta^{13}\mathrm{C}_{\mathrm{bb}} \times f_{\mathrm{bb}}(\mathrm{EC}) + \delta^{13}\mathrm{C}_{\mathrm{coal}} \times f_{\mathrm{coal}} + \delta^{13}\mathrm{C}_{\mathrm{vehicle}} \times f_{\mathrm{vehicle}}, \quad \text{(S2)}$$

$$f_{\mathrm{coal}} + f_{\mathrm{vehicle}} = f_{\mathrm{fossil}}\,(\mathrm{EC}), \quad \text{(S3)}$$

where $\delta^{13}C_{bb}$, $\delta^{13}C_{vehicle}$ and $\delta^{13}C_{coal}$ are the $\delta^{13}C$ signature of EC emitted from biomass burning, vehicle emissions and coal combustion, respectively. The means and the standard deviations for $\delta^{13}C_{bb}$ (-26.7 ± 1.8 ‰ for C3 plants), $\delta^{13}C_{vehicle}$ (-25.5 ± 1.3 ‰) and $\delta^{13}C_{coal}$ (-23.4 ± 1.3 ‰) are established in Andersson et al. (2015) by a thorough literature search and full compilation of $\delta^{13}C$ source signatures for EC. In brief, the mean and standard deviation for $\delta^{13}C$ endmembers for the different sources are estimated as the average and standard deviation of the different data sets,

respectively.

The source endmembers for $\delta^{13}C$ are less well-constrained than $f_{bb}(EC)$ and $f_{fossil}(EC)$, as $\delta^{13}C$ varies with fuel types and combustion conditions. For example, the range of possible $\delta^{13}C$ values for vehicle emission overlaps to a small extent with the range for coal combustion, although EC from vehicle emissions are usually more depleted than from coal combustion. Uncertainties of source signatures of $\delta^{13}C$ (i.e., $\delta^{13}C_{bb}$, $\delta^{13}C_{vehicle}$, $\delta^{13}C_{coal}$), the calculated $f_{fossil}(EC)$ derived from $F^{14}C_{EC}$, and the measured $\delta^{13}C_{EC}$ are propagated by the MCMC technique, where source signatures of $\delta^{13}C$ introduces a larger uncertainty than $f_{fossil}(EC)$ constrained by $F^{14}C$.

MCMC was implemented in the freely available R software (https://cran.r-project.org/), using the *simmr* package (https://CRAN.R-project.org/package=simmr). Convergence diagnostics were created to make sure the model has converged properly. The simulation for each sample was run with 10,000 iterations, using a burn-in of 1000 steps, and a data thinning of 100. The results of the MCMC are the posterior probability density functions (PDF) for the relative contributions from the sources (Fig. S3).

S3. Blank corrections for $F^{14}C$ of carbon fractions

The ^{14}C values of carbon fractions (i.e., mvOC, OC and EC) can be blank corrected accordioning to the mass balance equation:

$$F^{14}C_S = \frac{F^{14}C_m \times M_m - F^{14}C_b \times M_b}{M_m - M_b} \quad (S4)$$

where $F^{14}C_S$ is $F^{14}C$ of the aerosol carbon collected on the filter, which is blank corrected, $F^{14}C_m$ and M_m are the measured $F^{14}C$ and the measured mass of the respective carbon fraction (mvOC, OC or EC), and $F^{14}C_b$ and M_b the fraction modern and the mass of the respective carbon fraction of blanks.

Since the directly determined system blank (i.e. the amount of CO_2 measured, when no sample is introduced into the aerosol combustion system) is 0.52 ± 0.31 μgC mvOC per extraction (i.e., M_b for mvOC), it is much too small to be analyzed for $F^{14}C_b$ of mvOC. To do blank corrections for mvOC, we need to estimate its $F^{14}C_{b..}$ We assume that $F^{14}C_b$ for mvOC ranges from 0 to 1 with a continuous uniform distribution as the reviewer suggested. To propagate uncertainties, a Monte Carlo simulation with 10,000 individual calculations of $F^{14}C_S$ for mvOC was conducted according to Eq. (S4). For calculation inputs, $F^{14}C_b$ of mvOC. was randomly chosen from a

continuous uniform distribution between 0 and 1. $F^{14}C_m$ for mvOC was randomly chosen from a normal distribution symmetric around the measured values with uncertainties as standard deviation (Table S4). The random values for M_m and M_b were taken from a triangular distribution, which has its maximum at the central value and 0 at the upper and lower limits. Then 10,000 different estimations of $F^{14}C_S$ for mvOC were calculated. The derived average represents the best estimate, and the standard deviation represents the combined uncertainties.

Figure S9 shows the $F^{14}C$ of mvOC before and after blank corrections ($F^{14}C_m$ and $F^{14}C_s$, respectively) for the contamination introduced by the isolation procedure.

As shown in Figure S9, the differences in $F^{14}C$ values of mvOC before and after blank corrections are really small, with the biggest absolute difference of 0.009 for sample Taiyuan-L. The small correction of $F^{14}C$ for mvOC will not affect any conclusion from this study. Thus, in this study, the contamination is assessed but not used for further data correction.

For OC and EC, the contamination introduced by the isolation procedure yields 0.72 ± 0.44 μgC EC and 0.85 ± 0.49 μgC OC per extraction, respectively, which are the directly determined system blank (i.e. the amount of CO_2 measured, when no sample is introduced into the aerosol combustion system). The blanks are less than 3% of the sample amount and thus can be neglected, compared with our sample size of 30–391 μgC EC per extraction and 30–445 μgC OC per extraction. Therefore, the blank correction will not introduce large uncertainties to the data. In this study, the contamination is assessed but not used for further data correction for $F^{14}C$ of OC and EC.

S4. Gas-particle partitioning of OC fractions

Ambient OC has a large range of volatility and contains low to high volatility compounds. The low-volatility OC is in the particle phase, and high volatility OC is mostly in the gas phase. OC with intermediate volatility are semi-volatile (SVOC) and can either be in the particle or the gas phase depending on temperature, concentrations of OC etc. (Donahue et al., 2006, 2009).

In this study, particulate OC is collected on a single bare-quartz filter. mvOC (desorbed at 200 °C in He) on the quartz filters is influenced by evaporation of SVOC from collected particles and adsorption of organic vapors to the quartz fibers. To estimate the particulate fraction of mvOC, we estimate the gas-particle partitioning of individual OC fractions using the thermal/optical OC/EC analysis and a volatility basis set (VBS) model. The VBS bins the organic aerosol (OA) compounds according to the effective saturation concentrations (C^*). If we project concentrations

of organic aerosol (OA) onto the basis set of saturation concentrations, we can estimate the volatility distribution of the organic material. The concentrations of OA (C_{OA}) and the equilibrium partitioning fractions (f_i) at equilibrium can be described by (Donahue et al., 2006, 2011):

$$f_i = \left(1 + \frac{C_i^*}{C_{OA}}\right)^{-1} \quad \text{(S5)}$$

where C_i^* is the C^* for OC fraction i. If C_i^* is equal to C_{OA}, then 50 % of OA mass will be in the particle phase, that is $f_i = 0.5$; if $C_i^* = 4 \times C_{OA}$, then the OA is more volatile, and only 20 % OA mass in the particle phase ($f_i = 0.2$).

Thermal-optical OC/EC analysis measures OC, not the OA. We use the OA/OC mass ratio to estimate OA concentrations from the OC concentrations. Then Eq. S5 can be reformulated as:

$$X_{Pi} = \left(1 + \frac{C_i^*}{\frac{OA}{OC} \times C_{OC}}\right)^{-1} \quad \text{(S6)}$$

where X_{Pi} is the particulate fraction in OC fraction i; C_{OC} can be quantified by the thermal-optical OC/EC analysis, and is the sum of particulate OC fractions;

The C^* value for each OC fraction are taken from Ma et al. (2016), where OC fractions are measured using the IMPROVE_A protocol, and are derived so that X_{Pi} stands for the particulate fraction of the total carbon found on the filter for each temperature step i. The IMPROVE_A temperature plateaus in the pure He phase are 140 °C, 280 °C, 480 °C, 580 °C, and the corresponding thermal carbon fractions are called $OC_{140°C}$, $OC_{280°C}$, $OC_{480°C}$ and $OC_{580°C}$, where the subscript refers to the desorption temperature of the IMPROVE_A protocol, respectively. The empirical VBS consisting of bins separated by 0.5 of an order of magnitude in volatility at 300 K: the C^* for $OC_{140°C}$ to $OC_{580°C}$ are $10^{1.6}$, $10^{1.1}$, $10^{0.6}$ and $10^{0.1}$ μg m^{-3}, respectively. The OA/OC is assumed to be 1.8 for urban environment (Turpin and Lim, 2001; Xing et al., 2013). In this study, samples in Beijing, Guangzhou, Shanghai, Taiyuan and Chongqing are measured using the IMPROVE_A protocol, thus X_{pi} for samples of these five cities are estimated using the empirical C^*, as shown in Fig. 8a in the main text.

The particulate fraction (X_{pi}) of OC fractions increases considerably from $OC_{140°C}$ to $OC_{580°C}$, consistent with the temperature steps. The temperature of the OC/EC analysis is the desorption temperature rather than evaporation, but it is still reasonable to assume that the desorption temperature is closely related to the volatility. OC desorbed at higher temperature tends to have a low volatility and more likely to exist in the particle phase.

Increasing the particulate OC concentrations (C_{OC} in Eq. S6) increase the particulate fraction for each OC fraction ($X_{p1,}$ $X_{p2,}$ X_{p3} and X_{p4}). For example, when C_{OC} increases from 8.8 μg m^{-3} to 64 μg m^{-3}, particulate fraction of $OC_{140°C}$ increases from 0.28 (i.e., 28 % $OC_{140°C}$ in the particle phase) to 0.74 and particulate fraction of $OC_{280°C}$ increases from 0.56 to 0.90. The desorption temperature for mvOC is 200 °C, falling within the 140 °C for $OC_{140°C}$ and 280 °C for $OC_{280°C}$. We thus estimated the particulate fraction for mvOC will fall within the X_{p1} for $OC_{140°C}$ and X_{p2} for $OC_{280°C}$.

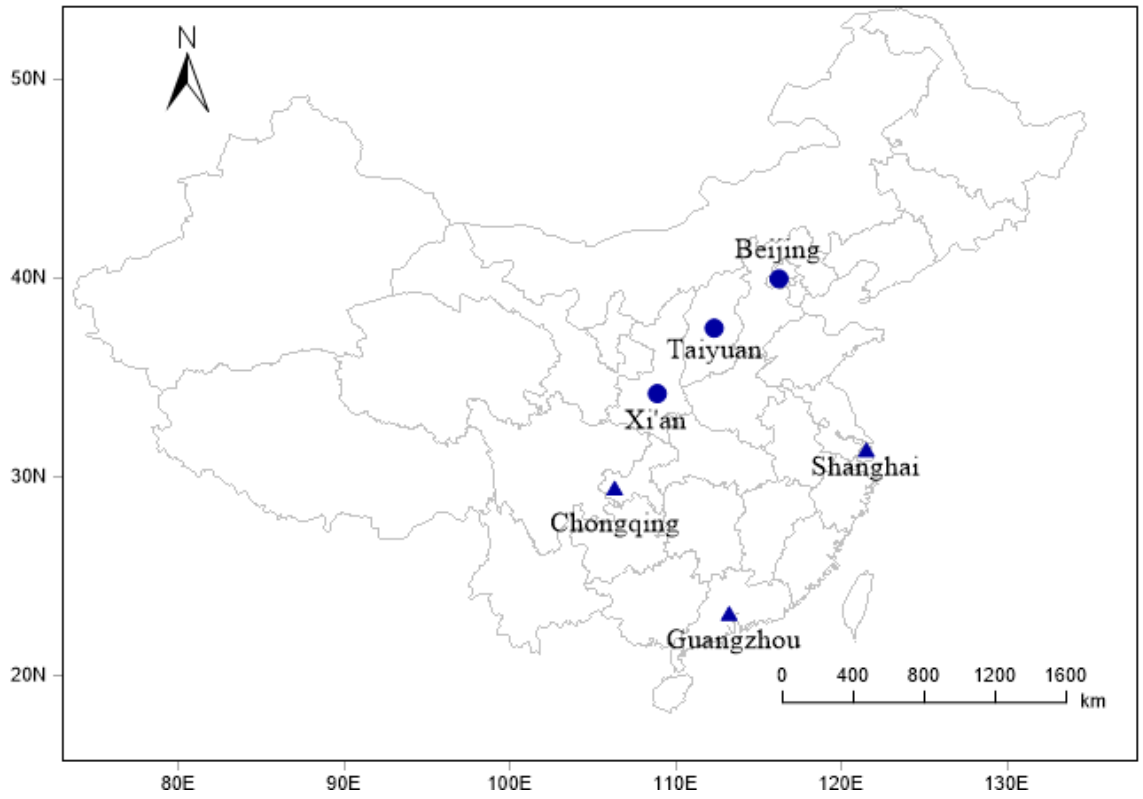

Figure S1. Geographic locations of the six Chinese sampling sites. Cities in northern China are shown as blue circle, cities in southern China as blue triangle. In northern China, large quantities of coal are used for heating during a formal residential "heating season" (15 November to 15 March next year) in winter.

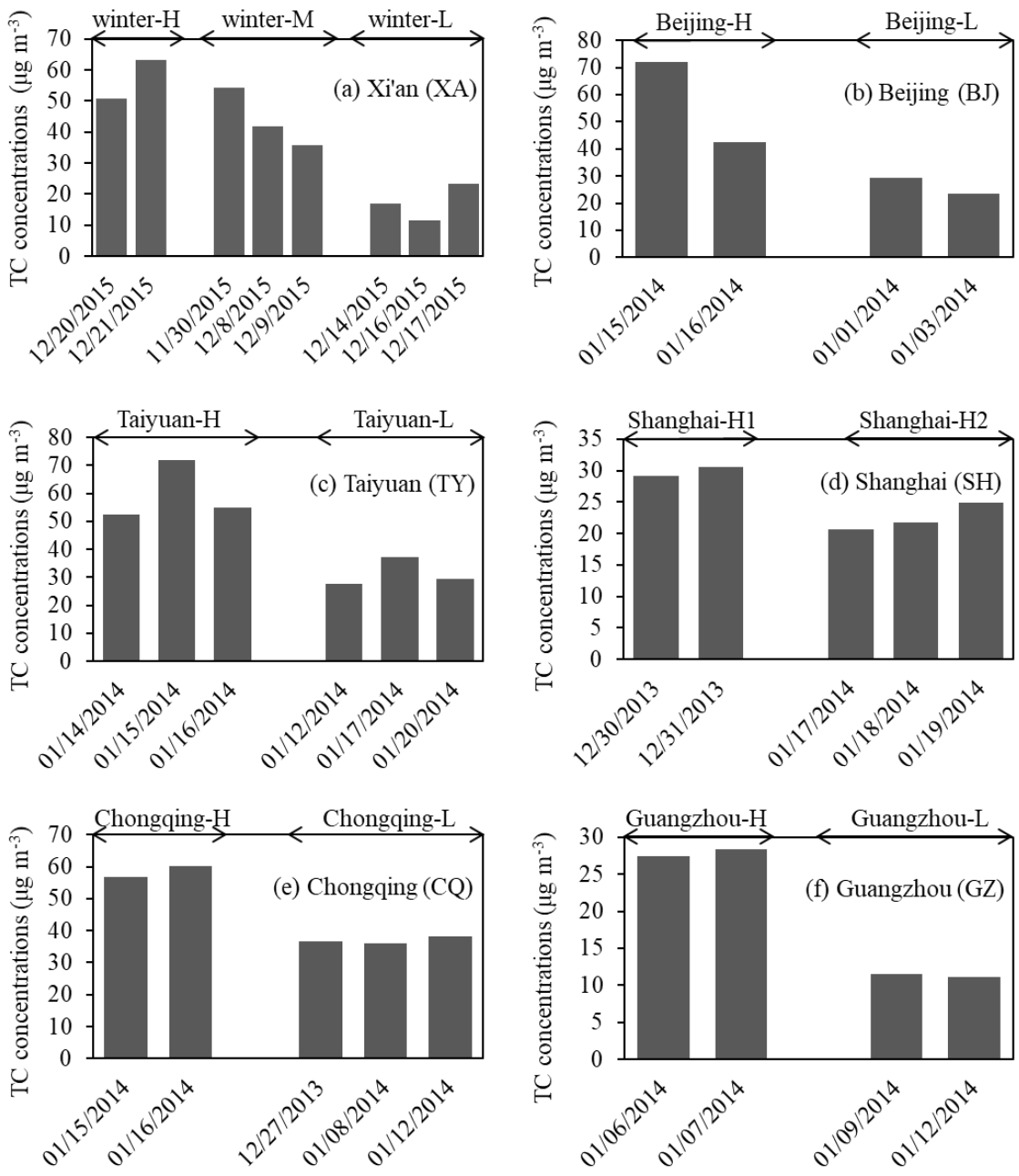

Figure S2. Selected samples for ^{14}C analysis. 2-3 composite samples that represent high (H), medium (M) and low (L) TC concentrations are combined from several individual filter samples for each city (a. Xi'an; b. Beijing; c. Taiyuan; d. Shanghai; e. Chongqing; f. Guangzhou). Each sample is consisting of 2 to 3 24-hr filter pieces with similar TC loadings and air mass backward trajectories (Table S1).

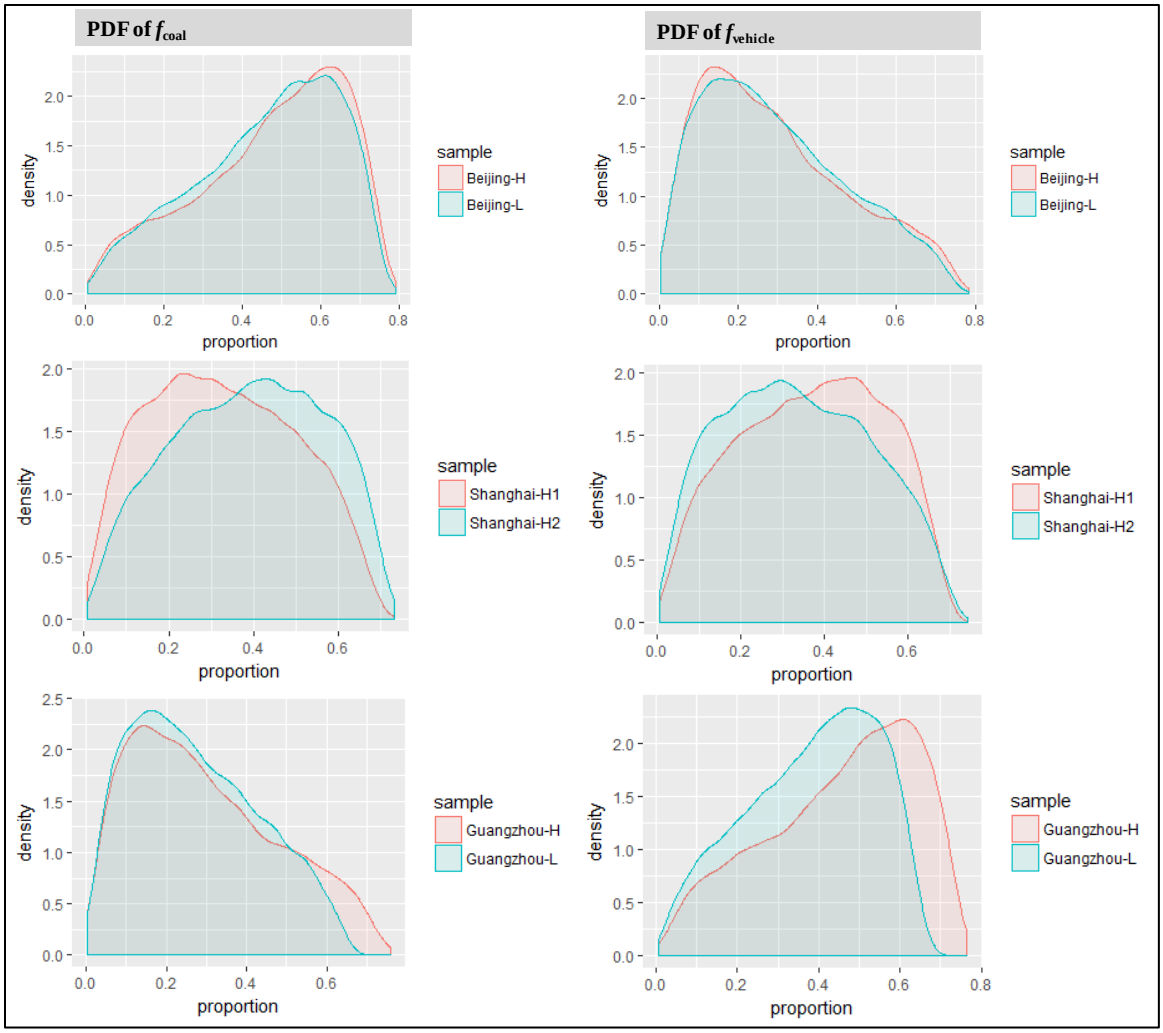

Figure S3. Probability density function **(**PDF) of the relative source contributions of coal and vehicle to EC (f_{coal}, $f_{vehicle}$) constrained by $\delta^{13}C$, calculated using the Bayesian Markov chain Monte Carlo approach (Supplement S2). Samples collected from other cities including Xi'an, Taiyuan, Chongqing were not measured for $\delta^{13}C_{EC}$.

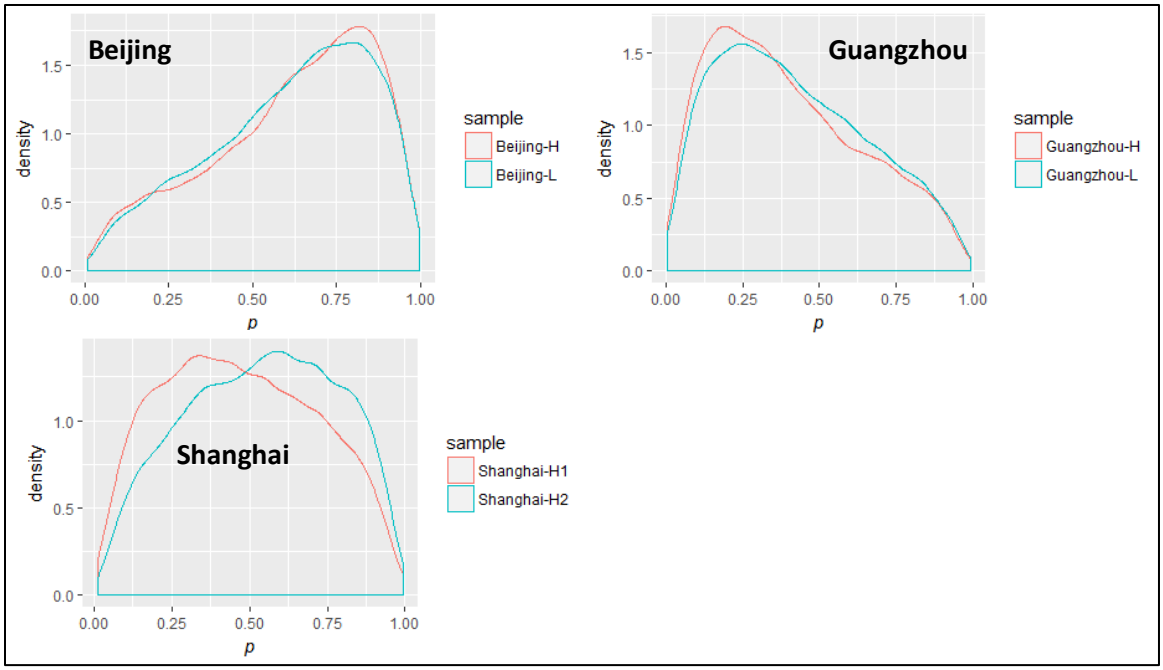

Figure S4. The PDF of *p* values (*p* is the fraction of EC from coal combustion in that from total fossil sources) for each sample, which is constrained by $\delta^{13}C_{EC}$. Calculation of *p* is present in Sect. 2.4. Other cities including Xi'an, Taiyuan, Chongqing were not measured for $\delta^{13}C$.

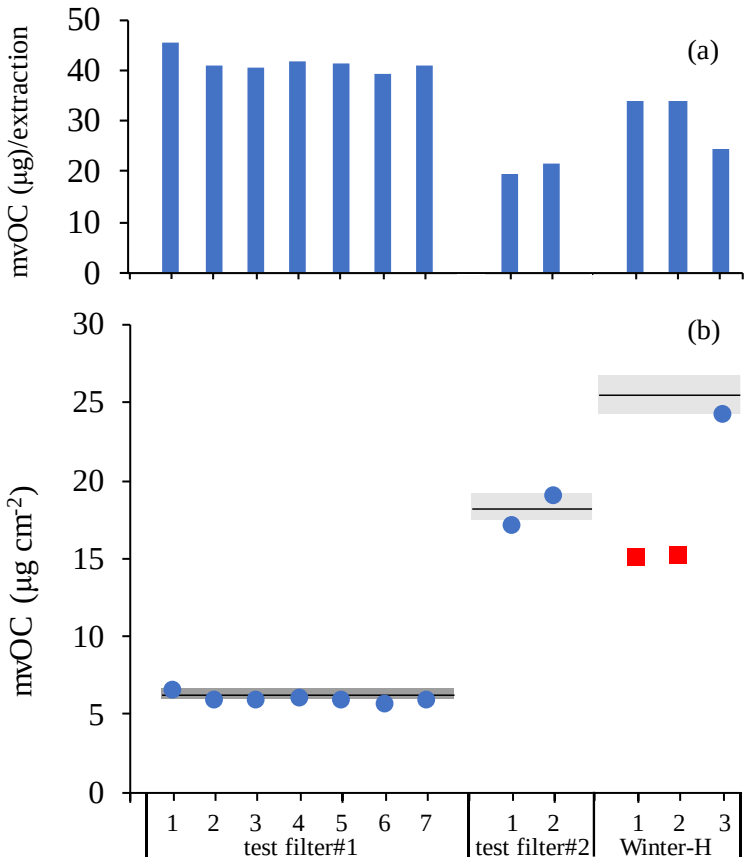

Figure S5. Reproducibility of desorption performed for test filter#1, test filter#2 and winter-H. The number on the *x*-axis represent the times of mvOC desorption. **(a)** the desorbed mvOC amount in µgC per extraction; **(b)** the desorbed mvOC in µg cm^{-2} calculated by dividing the desorbed mvOC amount (µgC) by the filter area (cm^2). The horizontal black line indicates the OC1 (µg cm^{-2}) measured by EUSAAR_2 protocol and the shaded area denotes its uncertainties. The two red squares represent the repeated mvOC extraction for sample winter-H using larger filter pieces. The panel (a) and (b) have the same *x*-axis.

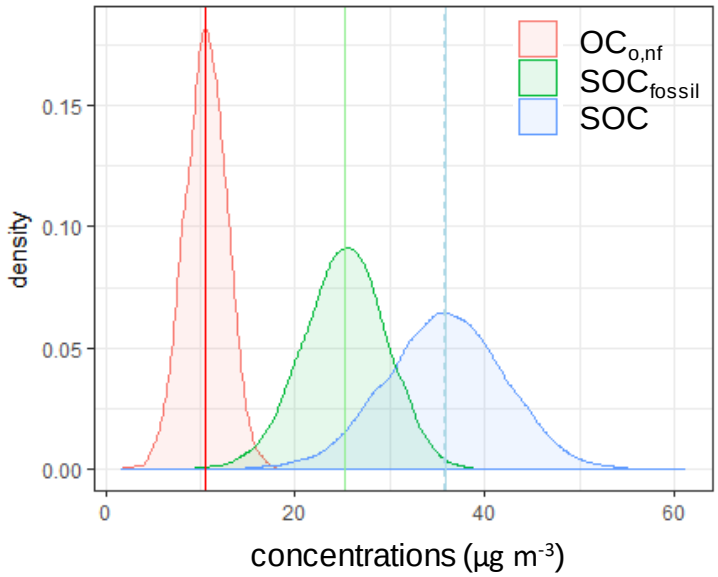

Figure S6. An example PDF of SOC concentrations (in light blue), SOC_{fossil} (light green) and $OC_{o.nf}$ (approximately SOC_{nf}, orange) for sample Beijing-H. The estimated SOC and SOC_{fossil} concentrations are estimated by ^{14}C-apportioned OC and EC in combination with *p* values randomly chosen from 0–1 (Sect. 2.4). The mean and median are indicated by the dashed and solid vertical lines. The mean and median are very close to each other due to the symmetric PDF. The median (interquartile range) and mean (± SD) values are given in Table S7 and Table S8, respectively.

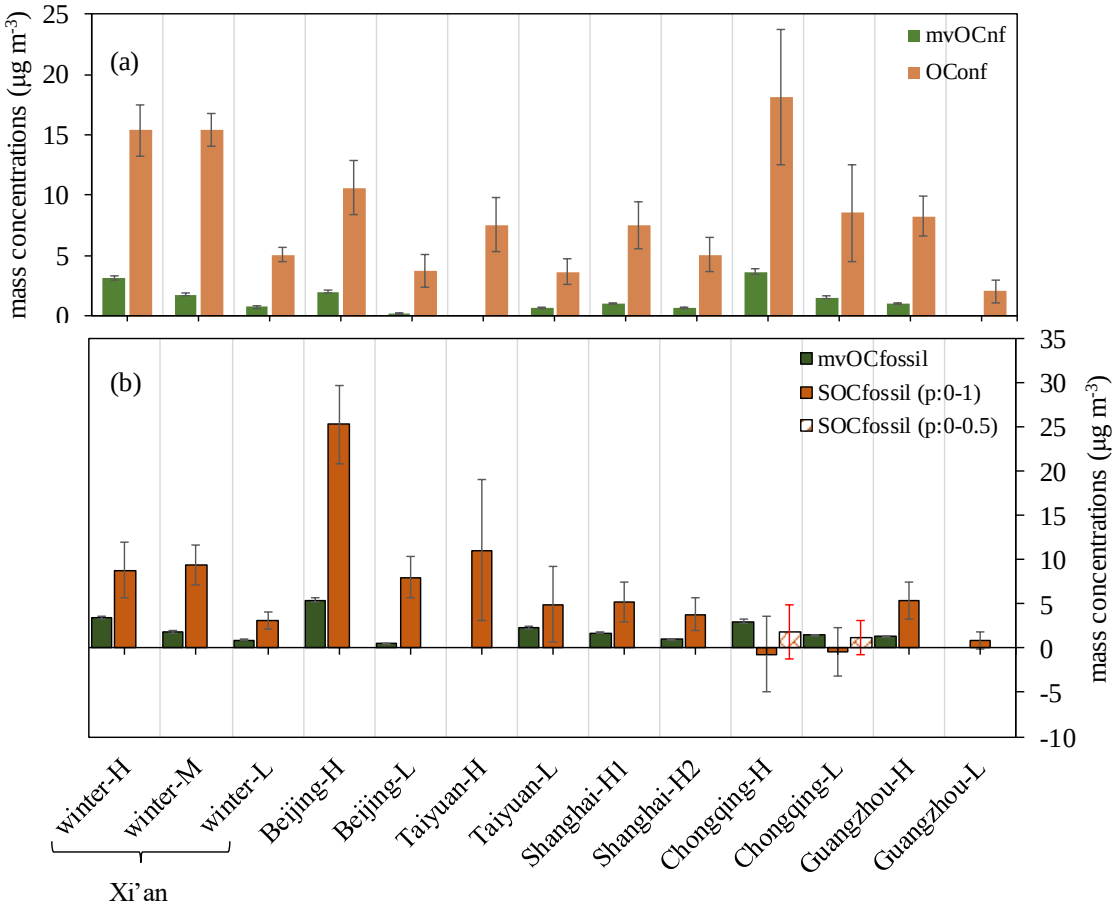

Figure S7. (a) Concentrations of $mvOC_{nf}$ (green bar) and $OC_{o,nf}$ (approximately SOC_{nf}, orange bar); **(b)** Concentrations of $mvOC_{fossil}$ (dark green bar), and SOC_{fossil}. SOC_{fossil} is estimated based on ^{14}C-apportioned OC and EC, combined with primary OC/EC ratios of coal combustion and vehicle exhaust, and *p* values. SOC_{fossil} estimated using using *p* values of 0–1 are shown in dark orange. For Chongqing, lower *p* values of 0–0.5 are used to estimate SOC_{fossil}, shown as bars filled with stripes. The panel (a) and (b) has the same *x*-axis.

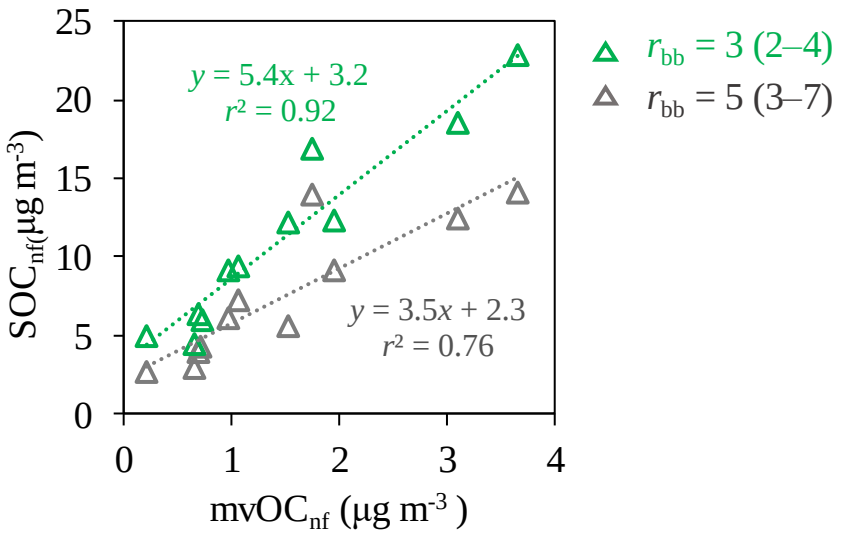

Figure S8. Correlation between $mvOC_{nf}$ and SOC_{nf}. SOC_{nf} is estimated by subtracting primary OC from biomass burning (POC_{bb}) from OC_{nf}, where POC_{bb} is estimated by multiplying EC_{bb} with the OC/EC ratio of fresh biomass burning plumes(r_{bb}). Here we take r_{bb}= 5 (3–7; mean; minimum-maximum) and r_{bb}= 3 (2–4), higher and lower than our best estimate of r_{bb} (4, 3–5), respectively.

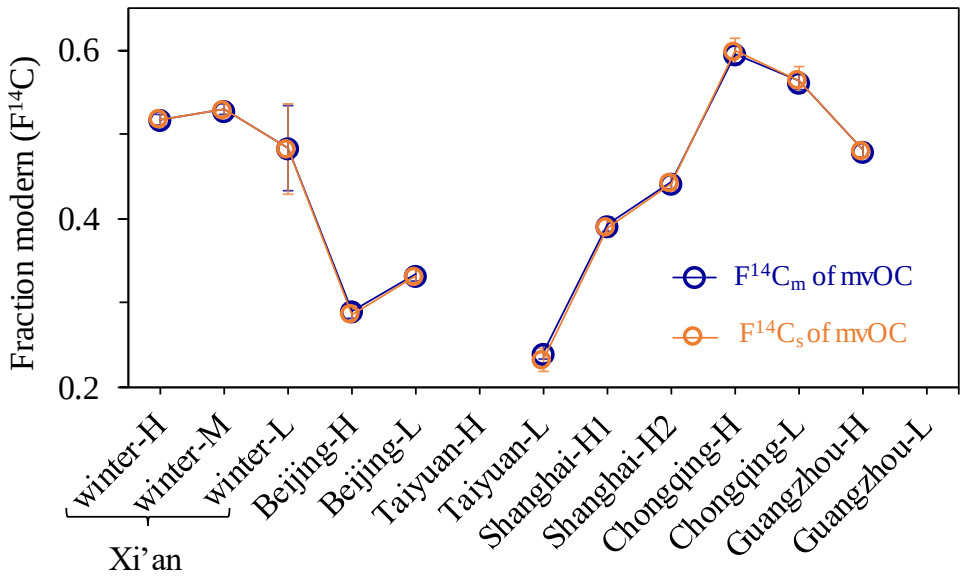

Figure S9. Fraction modern ($F^{14}C$) of mvOC before and after blank corrections ($F^{14}C_m$ and $F^{14}C_s$, respectively) for the contamination introduced by the isolation procedure. Detailed method to do the blank corrections is described in Supplement S3.

Table S1. Details of sampling information.

	City	Sampling sites	Longitude, latitude	Sample name*	Sampling date	RH (%)**	Temperature (°C)**	Wind speed (m s^{-1})**
Northern China	Xi'an (XA)	Institute of Earth Environment, Chinese Academy of Sciences	34.2° N, 108.9° E	winter-H	12/20/2015 12/21/2015	73 79	-3~6 -1~5	1.0 0.6
				winter-M	11/30/2015 12/8/2015 12/9/2015	 85 85	3~11 2~8 2~6	1.1 1.1 1.0
				winter-L	12/14/2015 12/16/2015 12/17/2015	67 50 65	-2~8 -5~4 -4~3	1.9 1.3 1.2
	Beijing (BJ)	Institute of Remote Sensing Applications, Chinese Academy of Sciences	39.9° N, 116.4° E	Beijing-H	1/15/2014 1/16/2014	56 67	-4~13 -3~5	1.5 1.9
				Beijing-L	1/1/2014 1/3/2014	37 50	-2~13 -4~8	1.6 2.2
	Taiyuan (TY)	Taiyuan University of Technology	37.9° N, 112.5° E	Taiyuan-H	1/14/2014 1/15/2014 1/16/2014	37 37 37	-14~3 -11~4 -13~5	1.3 1.2 1.2
				Taiyuan-L	1/12/2014 1/17/2014 1/20/2014	36 37 30	-15~2 -14~3 -14~3	1.2 1.6 2.5
Southern China	Shanghai (SH)	Fudan University	31.2° N, 121.4° E	Shanghai-H1	12/30/2013 12/31/2013	55 49	-3~10 -1~14	1.8 2.0
				Shanghai-H2	1/17/2014 1/18/2014 1/19/2014	70 76 67	5~11 -2~7 3~10	2.4 1.8 2.5
	Chongqing (CQ)	Super Monitoring Station of Chongqing	29.9° N, 106.5° E	Chongqing-H	1/15/2014 1/16/2014	86 91	7~9 7~10	0.5 0.2
				Chongqing-L	12/27/2013 1/8/2014 1/12/2014	92 90 89	6~9 6~8 4~10	0.4 0.3 0.5
	Guangzhou (GZ)	South China Institute of Environmental Sciences, Ministry of Environment Protection	23.1° N, 113.2° E	Guangzhou-H	1/6/2014 1/7/2014	73 84	11~20 16~21	1.6 1.7
				Guangzhou-L	1/9/2014 1/12/2014	62 67	11~15 8~18	2.8 4.9

*Composite samples that represent high (H), medium(M) and low (L) TC concentrations are combined from several individual 24-hr samples for ^{14}C analysis.
**The meteorological data is obtained from the Meteorological Institute of Shaanxi Province, Xi'an, China. Daily average relative humidity (RH), daily average wind speed (m s-1) and ambient temperature (minimum~maximum; °C). There was no precipitation in all cities during all sampling dates.

Table S2. Pilot tests to determine the flushing time using He before heating the filter pieces at 200 °C in He to desorb mvOC, using a test filter. The results show that the flushing time (10 min, 15 min or 60 min) does not affect the desorption amount of mvOC.

Test	Flushing time	Desorbed amount of mvOC
1	10 min	5.8 μg cm^{-2}
2	15 min	5.9 μg cm^{-2}
3	15 min	5.8 μg cm^{-2}
4	60 min	5.7 μg cm^{-2}
5	60 min	5.7 μg cm^{-2}

Table S3. Measured $F^{14}C$ values and masses of the standards with their nominal $F^{14}C$ values.

Standards		nominal $F^{14}C$	measured $F^{14}C$ ($F^{14}C_m$)	measured mass (M_m, μgC)
Combustion processes[a]	OXII	1.3406	1.327 ± 0.022	65
	OXII	1.3406	1.321 ± 0.012	117
	anthracite	0	0.020 ± 0.001	51
	anthracite	0	0.002 ± 0.001	75
	anthracite	0	0.008 ± 0.001	217
	anthracite	0	0.004 ± 0.001	219
	anthracite	0	0.005 ± 0.001	254

[a] For combustion processes, two sets of standard material: the oxalic acid HOxII and anthracite with known ^{14}C contents ($F^{14}C$ = 1.3406 and $F^{14}C$ = 0, respectively) were combusted using the aerosol combustion system (ACS) and used for quality control.

Table S4. Concentrations of mvOC, OC and EC (μg m^{-3}), the contribution of mvOC to the total OC (mvOC/OC, %), fraction modern of mvOC, OC and EC ($F^{14}C_{(mvOC)}$, $F^{14}C_{(OC)}$, $F^{14}C_{(EC)}$) and stable carbon isotopic composition of EC ($\delta^{13}C_{EC}$).

City	Sample Name	mvOC* (μg m^{-3})	OC (μg m^{-3})	EC (μg m^{-3})	mvOC/OC (%)	$F^{14}C_{(mvOC)}$	$F^{14}C_{(OC)}$	$F^{14}C_{(EC)}$	$\delta^{13}C_{EC}$ (‰)
Xi'an (XA)	winter-H	6.5	47.1	9.9	13.9	0.517 ± 0.006	0.640 ± 0.009	0.340 ± 0.005	
	winter-M	3.6	37.9	6.1	9.5	0.529 ± 0.007	0.609 ± 0.007	0.258 ± 0.005	
	winter-L	1.6	14.5	2.8	11.2	0.483 ± 0.050**	0.626 ± 0.007	0.320 ± 0.005	
Beijing (BJ)	Beijing-H	7.4	50.4	6.9	14.6	0.290 ± 0.008	0.366 ± 0.003	0.253 ± 0.002	-23.96 ± 0.02
	Beijing-L	0.7	21.8	4.7	3.3	0.334 ± 0.008	0.413 ± 0.004	0.266 ± 0.003	-24.06 ± 0.02
Taiyuan (TY)	Taiyuan-H	2.4	45.1	14.8	5.3	NA***	0.320 ± 0.030	0.106 ± 0.002	
	Taiyuan-L	2.9	23.2	8.2	12.7	0.241 ± 0.008	0.318 ± 0.023	0.105 ± 0.003	
Shanghai (SH)	Shanghai-H1	2.7	24.7	5.2	10.9	0.392 ± 0.008	0.609 ± 0.004	0.332 ± 0.003	-25.45 ± 0.03
	Shanghai-H2	1.7	18.2	4.2	9.3	0.443 ± 0.008	0.580 ± 0.004	0.303 ± 0.003	-24.72 ± 0.02
Chongqing (CQ)	Chongqing-H	6.7	46.7	11.8	14.3	0.595 ± 0.011	0.839 ± 0.029	0.414 ± 0.010	
	Chongqing-L	3	29	8.1	10.2	0.562 ± 0.010	0.833 ± 0.028	0.466 ± 0.026	
Guangzhou (GZ)	Guangzhou-H	2.4	23.4	4.5	10.3	0.481 ± 0.008	0.592 ± 0.004	0.271 ± 0.002	-26.01 ± 0.02
	Guangzhou-L	1	8.8	2.5	10.9	NA***	0.667 ± 0.005	0.375 ± 0.004	-26.15 ± 0.02

* Excellent agreement was found between mvOC amount measured using ACS system and OC1 following EUSAAR_2 using a Sunset carbon analyzer, except for sample winter-L. Here we took the OC1 by EUSAAR_2 as mvOC concentrations (both desorbed at 200 °C in He) for samples at Xi'an. Blank corrections were performed for OC1 mass, the mvOC concentrations in Xi'an were therefore blank corrected. ** For sample winter-L, we take the measured $F^{14}C_{(mvOC)}$ values but assign a bigger absolute uncertainty of 0.05, due to their low mvOC recoveries. *** Samples get lost during the ^{14}C measurements.

Table S5. Relative non-fossil sources contribution to mvOC, OC, EC and mrOC (f_{nf}(mvOC), f_{nf}(OC), f_{bb}(EC), f_{nf}(mrOC)), and relative fossil sources contribution to mvOC, OC, EC and mrOC(f_{fossil}(mvOC), f_{fossil}(OC), f_{fossil}(EC), f_{fossil}(mrOC)).

City	Sample Name	f_{nf}(mvOC)	f_{nf}(OC)	f_{bb}(EC)	f_{nf}(mrOC)*	f_{fossil}(mvOC)	f_{fossil}(OC)	f_{fossil}(EC)	f_{fossil}(mrOC)*
Xi'an	winter-H	0.475 ± 0.011	0.587 ± 0.014	0.309 ± 0.008	0.606 ± 0.015	0.525 ± 0.011	0.413 ± 0.014	0.691 ± 0.008	0.394 ± 0.015
(XA)	winter-M	0.485 ± 0.011	0.558 ± 0.012	0.235 ± 0.006	0.566 ± 0.013	0.515 ± 0.011	0.442 ± 0.012	0.765 ± 0.006	0.434 ± 0.013
	winter-L	0.443 ± 0.047	0.574 ± 0.012	0.291 ± 0.007	0.591 ± 0.014	0.557 ± 0.047	0.426 ± 0.012	0.709 ± 0.007	0.409 ± 0.014
Beijing	Beijing-H	0.266 ± 0.009	0.336 ± 0.007	0.230 ± 0.005	0.348 ± 0.008	0.734 ± 0.009	0.664 ± 0.007	0.770 ± 0.005	0.652 ± 0.008
(BJ)	Beijing-L	0.306 ± 0.009	0.379 ± 0.008	0.242 ± 0.005	0.382 ± 0.008	0.694 ± 0.009	0.621 ± 0.008	0.758 ± 0.005	0.618 ± 0.008
Taiyuan	Taiyuan-H	NA**	0.293 ± 0.028	0.096 ± 0.003	NA	NA	0.707 ± 0.028	0.904 ± 0.003	NA
(TY)	Taiyuan-L	0.221 ± 0.009	0.292 ± 0.022	0.095 ± 0.003	0.302 ± 0.025	0.779 ± 0.009	0.708 ± 0.022	0.905 ± 0.003	0.698 ± 0.025
Shanghai	Shanghai-H1	0.360 ± 0.010	0.559 ± 0.011	0.302 ± 0.006	0.584 ± 0.012	0.640 ± 0.010	0.441 ± 0.011	0.698 ± 0.006	0.416 ± 0.012
(SH)	Shanghai-H2	0.406 ± 0.011	0.532 ± 0.011	0.275 ± 0.006	0.545 ± 0.011	0.594 ± 0.011	0.468 ± 0.011	0.725 ± 0.006	0.455 ± 0.011
Chongqing	Chongqing-H	0.546 ± 0.014	0.771 ± 0.030	0.377 ± 0.011	0.809 ± 0.035	0.454 ± 0.014	0.229 ± 0.030	0.623 ± 0.011	0.191 ± 0.035
(CQ)	Chongqing-L	0.516 ± 0.014	0.764 ± 0.030	0.423 ± 0.025	0.794 ± 0.033	0.484 ± 0.014	0.236 ± 0.030	0.577 ± 0.025	0.206 ± 0.033
Guangzhou	Guangzhou-H	0.441 ± 0.011	0.543 ± 0.011	0.246 ± 0.005	0.555 ± 0.011	0.559 ± 0.011	0.457 ± 0.011	0.754 ± 0.005	0.445 ± 0.011
(GZ)	Guangzhou-L	NA**	0.612 ± 0.012	0.341 ± 0.007	NA	NA	0.388 ± 0.012	0.659 ± 0.007	NA

* f_{nf}(mrOC) is calculated by the differences between OC and mvOC (Sect. 2.4); ** Samples get lost during the ^{14}C measurements.

Table S6. Concentrations of mvOC, OC and EC from non-fossil sources ($mvOC_{nf}$, OC_{nf} and EC_{bb}) and fossil sources ($mvOC_{fossil}$, OC_{fossil} and EC_{fossil}) in units of μg m^{-3}.

City	Sample Name	$mvOC_{nf}$	$mvOC_{fossil}$	OC_{nf}	OC_{fossil}	EC_{bb}	EC_{fossil}
Xi'an	winter-H	3.11 ± 0.19	3.44 ± 0.21	27.69 ± 1.53	19.46 ± 1.17	3.08 ± 0.18	6.86 ± 0.37
(XA)	winter-M	1.74 ± 0.11	1.85 ± 0.12	21.15 ± 1.17	16.73 ± 0.97	1.44 ± 0.09	4.70 ± 0.26
	winter-L	0.72 ± 0.09	0.91 ± 0.10	8.32 ± 0.47	6.17 ± 0.37	0.82 ± 0.05	1.99 ± 0.12
Beijing	Beijing-H	1.96 ± 0.12	5.41 ± 0.28	16.91 ± 1.73	33.47 ± 3.37	1.58 ± 0.32	5.29 ± 1.06
(BJ)	Beijing-L	0.22 ± 0.01	0.49 ± 0.03	8.25 ± 0.84	13.49 ± 1.36	1.13 ± 0.23	3.55 ± 0.73
Taiyuan	Taiyuan-H	NA	NA	13.22 ± 1.85	31.86 ± 3.42	1.42 ± 0.29	13.38 ± 2.69
(TY)	Taiyuan-L	0.65 ± 0.04	2.29 ± 0.12	6.76 ± 0.84	16.42 ± 1.72	0.78 ± 0.16	7.40 ± 1.48
Shanghai	Shanghai-H1	0.97 ± 0.06	1.72 ± 0.09	13.79 ± 1.40	10.88 ± 1.13	1.58 ± 0.32	3.64 ± 0.73
(SH)	Shanghai-H2	0.69 ± 0.04	1.01 ± 0.05	9.71 ± 0.99	8.54 ± 0.87	1.16 ± 0.23	3.05 ± 0.61
Chongqing	Chongqing-H	3.66 ± 0.21	3.04 ± 0.18	35.97 ± 3.89	10.73 ± 1.76	4.44 ± 0.90	7.34 ± 1.47
(CQ)	Chongqing-L	1.53 ± 0.09	1.43 ± 0.08	22.14 ± 2.39	6.81 ± 1.11	3.39 ± 0.70	4.62 ± 0.94
Guangzhou	Guangzhou-H	1.06 ± 0.06	1.34 ± 0.07	12.70 ± 1.29	10.66 ± 1.09	1.11 ± 0.22	3.40 ± 0.68
(GZ)	Guangzhou-L	NA	NA	5.39 ± 0.54	3.43 ± 0.36	0.84 ± 0.17	1.62 ± 0.32

Table S7. Concentrations of SOC, SOC from fossil sources (SOC_{fossil}) and OC from non-fossil sources excluding primary biomass burning ($OC_{o,nf}$) and fraction of fossil in SOC (f_{fossil}(SOC)) (median and interquartile range).

City	Sample Name	f_{fossil}(SOC)			SOC concentrations (μg m^{-3})		
		p (0–1)[a]	^{13}C-constrained *p*[b]	*p* (0–0.5)[c]	*p* (0–1)	^{13}C-constrained *p*	*p* (0–0.5)
Xi'an (XA)	winter-H	0.37 (0.29–0.42)			24.25 (21.41–27.10)		
	winter-M	0.38 (0.34–0.42)			24.83 (22.79–26.84)		
	winter-L	0.38 (0.32–0.43)			8.15 (7.28–8.99)		
Beijing (BJ)	Beijing-H	0.70 (0.68–0.72)	0.70 (0.68–0.71)		36.01 (31.67–40.13)	35.20 (32.75–37.82)	
	Beijing-L	0.68 (0.64–0.72)	0.67 (0.63–0.70)		11.80 (9.48–14.06)	11.49 (9.99–12.78)	
Taiyuan (TY)	Taiyuan-H	0.61 (0.47–0.69)			19.13 (12.56–24.90)		
	Taiyuan-L	0.61 (0.44–0.69)			8.88 (5.30–12.04)		
Shanghai (SH)	Shanghai-H1	0.41 (0.35–0.47)	0.43 (0.38–0.46)		12.87 (10.22–15.36)	12.85 (11.28–14.38)	
	Shanghai-H2	0.43 (0.35–0.49)	0.42 (0.36–0.47)		8.96 (6.87–10.87)	8.74 (7.44–9.90)	
Chongqing (CQ)	Chongqing-H	-0.01 (-0.23–0.12)		0.10 (0–0.17)	17.70 (12.03–23.06)		20.20 (15.05–25.20)
	Chongqing-L	0.04 (-0.25–0.19)		0.14 (0.02–0.22)	8.34 (4.50–12.06)		9.84 (6.25–13.31)
Guangzhou (GZ)	Guangzhou-H	0.40 (0.34–0.45)	0.43 (0.39–0.46)		13.69 (11.37–15.96)	14.30 (12.93–15.50)	
	Guangzhou-L	0.34 (0.18–0.44)	0.36 (0.25–0.44)		2.99 (1.84–4.06)	3.15 (2.49–3.79)	

Table S7. Continued

City	Sample Name	SOC_{fossil}			$OC_{o,nf}$ (approximately SOC_{nf})
		p (0–1)	^{13}C-constrained *p*	*p* (0–0.5)	
Xi'an (XA)	winter-H	8.86 (6.49–11.28)			15.42 (13.98–16.82)
	winter-M	9.46 (7.77–11.13)			15.38 (14.46–16.31)
	winter-L	3.10 (2.37–3.80)			5.05 (4.64–5.48)
Beijing (BJ)	Beijing-H	25.41 (22.33–28.29)	24.55 (22.69–26.58)		10.60 (9.13–12.15)
	Beijing-L	8.09 (6.45–9.66)	7.63 (6.60–8.82)		3.74 (2.82–4.63)
Taiyuan (TY)	Taiyuan-H	11.63 (5.74–16.78)			7.49 (6.02–9.01)
	Taiyuan-L	5.27 (2.05–8.07)			3.64 (2.90–4.39)
Shanghai (SH)	Shanghai-H1	5.36 (3.78–6.85)	5.39 (4.23–6.45)		7.54 (6.19–8.88)
	Shanghai-H2	3.92 (2.60–5.11)	3.62 (2.72–4.55)		5.07 (4.12–6.05)
Chongqing (CQ)	Chongqing-H	-0.37 (-3.58–2.38)		2.00 (-0.10–3.91)	18.24 (14.51–21.93)
	Chongqing-L	-0.16 (-2.14–1.58)		1.27 (0.03–2.52)	8.65 (5.94–11.27)
Guangzhou (GZ)	Guangzhou-H	5.52 (3.99–6.87)	6.12 (5.10–6.95)		8.26 (7.16–9.37)
	Guangzhou-L	0.99 (0.28–1.57)	1.19 (0.68–1.56)		2.06 (1.41–2.67)

[a] *p* is the contribution of coal combustion to fossil EC (Eq. 12), *p* was randomly chosen from 0–1, that is no constrains on *p* values.
[b] Samples taken from Beijing, Shanghai and Guangzhou were measured for both $F^{14}C_{(EC)}$ and $\delta^{13}C_{EC}$, and *p* in these three cities is further constrained by $\delta^{13}C_{EC}$ (Supplement S2).
[c] For Chongqing, we did a sensitive analysis for *p* and tried a smaller *p* of 0–0.5.

Table S8. Concentrations of SOC, SOC from fossil sources (SOC_{fossil}) and non-fossil sources ($OC_{o,nf}$) and fraction of fossil in SOC ($f_{fossil}(SOC)$) (μg m^{-3}; mean ± standard deviation).

City	Sample Name	SOC concentrations		SOC_{fossil}		$OC_{o,nf}$ (approximately SOC_{nf})
		p (0–1)[a]	*p* (0–0.5)[b]	*p* (0–1)	*p* (0–0.5)	
Xi'an (XA)	winter-H	24.17 ± 4.12		8.79 ± 3.17		15.38 ± 2.13
	winter-M	24.79 ± 2.91		9.41 ± 2.25		15.38 ± 1.36
	winter-L	8.13 ± 1.24		3.08 ± 0.94		5.05 ± 0.61
Beijing (BJ)	Beijing-H	35.87 ± 6.29		25.26 ± 4.40		10.61 ± 2.24
	Beijing-L	11.67 ± 3.36		7.96 ± 2.33		3.71 ± 1.32
Taiyuan (TY)	Taiyuan-H	18.56 ± 9.12		11.02 ± 7.96		7.54 ± 2.26
	Taiyuan-L	8.60 ± 4.90		4.94 ± 4.27		3.65 ± 1.11
Shanghai (SH)	Shanghai-H1	12.75 ± 3.80		5.24 ± 2.22		7.51 ± 1.98
	Shanghai-H2	8.84 ± 2.97		3.78 ± 1.85		5.05 ± 1.44
Chongqing (CQ)	Chongqing-H	17.40 ± 8.33	20.0 ± 7.6	-0.72 ± 4.28	1.80 ± 3.04	18.12 ± 5.59
	Chongqing-L	8.13 ± 5.65	9.8 ± 5.1	-0.38 ± 2.71	1.23± 1.90	8.51 ± 3.97
Guangzhou (GZ)	Guangzhou-H	13.62 ± 3.39		5.38 ± 2.10		8.25 ± 1.64
	Guangzhou-L	2.95 ± 1.67		0.90 ± 0.93		2.04 ± 0.94

[a] *p* is the contribution of coal combustion to fossil EC (Eq. 12), *p* was randomly chosen from 0–1, that is no constrains on *p* values.
[b] For Chongqing, we did a sensitive analysis for *p* and tried a smaller *p* of 0–0.5.

References

Andersson, A., Deng, J., Du, K., Zheng, M., Yan, C., Sköld, M., and Gustafsson, Ö.: Regionally-varying combustion sources of the January 2013 severe haze events over eastern China, Environ. Sci. Technol., 49, 2038–2043, 2015.

Cao, J.-j., Chow, J. C., Tao, J., Lee, S.-c., Watson, J. G., Ho, K.-f., Wang, G.-h., Zhu, C.-s., and Han, Y.-m.: Stable carbon isotopes in aerosols from Chinese cities: Influence of fossil fuels, Atmos. Environ., 45, 1359-1363, http://dx.doi.org/10.1016/j.atmosenv.2010.10.056, 2011.

Donahue, N. M., Robinson, A. L., Stanier, C. O., and Pandis, S. N.: Coupled Partitioning, Dilution, and Chemical Aging of Semivolatile Organics, Environ. Sci. Technol., 40, 2635-2643, 2006.

Donahue, N. M., Robinson, A. L., and Pandis, S. N.: Atmospheric organic particulate matter: From smoke to secondary organic aerosol, Atmos. Environ., 43, 94-106, http://dx.doi.org/10.1016/j.atmosenv.2008.09.055, 2009.

Donahue, N. M., Epstein, S. A., Pandis, S. N., and Robinson, A. L.: A two-dimensional volatility basis set: 1. organic-aerosol mixing thermodynamics, Atmos. Chem. Phys., 11, 3303-3318, https://doi.org/10.5194/acp-11-3303-2011, 2011.

Ma, J., Li, X., Gu, P., Dallmann, T. R., Presto, A. A., and Donahue, N. M.: Estimating ambient particulate organic carbon concentrations and partitioning using thermal optical measurements and the volatility basis set, Aerosol Sci. Technol., 50, 638-651, 2016.

Ni, H., Huang, R.-J., Cao, J., Liu, W., Zhang, T., Wang, M., Meijer, H. A. J., and Dusek, U.: Source apportionment of carbonaceous aerosols in Xi'an, China: insights from a full year of measurements of radiocarbon and the stable isotope ^{13}C, Atmos. Chem. Phys., 18, 16363-16383, https://doi.org/10.5194/acp-18-16363-2018, 2018.

Turpin, B. J., and Lim, H.-J.: Species contributions to $PM_{2.5}$ mass concentrations: revisiting common assumptions for estimating organic mass, Aerosol Sci. Technol., 35, 602-610, 2001.

Xing, L., Fu, T.-M., Cao, J. J., Lee, S. C., Wang, G. H., Ho, K. F., Cheng, M.-C., You, C.-F., and Wang, T. J.: Seasonal and spatial variability of the OM/OC mass ratios and high regional correlation between oxalic acid and zinc in Chinese urban organic aerosols, Atmos. Chem. Phys., 13, 4307-4318, https://doi.org/10.5194/acp-13-4307-2013, 2013.